CFD ANALYSIS OF INCOMPRESSIBLE TURBULENT FLOW PROBLEMS USING UNSTEADY RANS AND LARGE EDDY SIMULATION APPROACH

Sekhar Majumdar[1] B.N.Rajani[2] D.S.Kulkarni[2] M.B.Subrahmanya[2]

[1]Former Head, Computational and Theoretical Fluid Dynamics Division
National Aerospace Laboratories (CSIR), Bangalore 560 017, India

[2]Scientist, CTFD Division, NAL (CSIR) Bangalore 560 017, India

ABSTRACT

The present paper focuses on the recent development of an implicit pressure-based finite volume algorithm for numerical solution of Navier Stokes equation in an inertial frame of reference for prediction of unsteady incompressible flow problems. The algorithm uses boundary-conforming, multiblock structured grid with moving boundaries, collocated variable arrangement with momentum equations resolved along cartesian directions, second order accurate spatial and temporal discretisation schemes for the convective fluxes and a pressure-velocity solution strategy. Effect of turbulence is simulated using one of the two different approaches. In the Unsteady Reynolds Averaged (URANS) approach coupled to appropriate eddy viscosity based turbulence models, the Navier Stokes (NS) equations, averaged over the whole range of turbulent length scales of the flow, are solved numerically. On the other hand, in the Large Eddy Simulation (LES) approach, the model filtered 3D NS equations are directly solved for the flow variables to resolve the large scale turbulent motions whereas the transport processes at the fine subgrid scale level only are simulated using simple algebraic turbulence model. The capabilities and limitations of both the cost-effective URANS approach and the relatively expensive but rich in physics LES approach have been demonstrated for few application problems of engineering interest.

Key Words : *Multiblock Boundary-Conforming Grid, Moving Boundary, Pressure-Velocity solution strategy, Eddy viscosity based Turbulence Models, Unsteady Flow, Large Eddy Simulation, Smagorinsky's SGS model*

1. INTRODUCTION

The recent advances of CFD in the area of incompressible flows are gradually proving to be invaluable asset for design and analysis of complex problems in the area of hydrodynamics as well as low speed aerodynamics. Some important examples include design of ships, submarines, underwater missiles, off-shore structures, commercial transport aircraft, automobiles *etc.*. Accurate prediction of turbulent flow around complex shaped structures is of practical interest in the calculation of the drag resistance of the body, in the design of propellers and other appendages, in the analysis of flow-induced noise and finally in the determination of the ensuing wake behind the structure.

Specially numerical simulation of unsteady flows with one or more moving boundaries are of great interest for the designers to understand the dynamics of various complex flow situations like the behaviour of an aircraft or a naval vessel during maneuvers. In these applications, flows are highly non-linear due to unsteadiness, flow separation, viscous/inviscid, vortex/body or vortex/vortex kind of interactions, transition to turbulence or relaminarisation. Extensive research therefore continues along various fronts to fully integrate CFD capabilities into the design process of ship, automobiles or low speed transport aircraft. However, considering the constraint of computing resources, Unsteady Reynolds Averaged Navier Stokes (URANS) methodology coupled to appropriate turbulence models, is often used in practice as the most cost-effective approach to predict the mean flow characteristics of the complex turbulent flow systems. Two major arguments against the use of URANS procedure are the loss of many important details of turbulence interaction due to Reynolds averaging and also that almost all the eddy viscosity based turbulence models have been designed and calibrated on the basis of mean flow parameters of turbulent shear flows only**.** On the other hand, in the moderately expensive Large Eddy Simulation (LES) approach, the complex physics of turbulent flow is resolved more

[1] *Professor, Dept. of Mech. Engg, Nitte Meenakshi Institute of Technology, Bangalore 560 064, India, Consultant CFD, Fluidyn Software & Consultancies Pvt. Ltd.*
e-mail address : essem17@gmail.com

accurately since the motion of the large scale flow structures involved in momentum and energy transfer processes are resolved numerically from the 3D unsteady NS equations and the effect of the smallest fine scales of turbulence only are modeled. The present paper provides a very brief overview of the work carried out at the CTFD Division, NAL Bangalore, by the research group of the first author during the last fifteen years on the development of a robust and accurate general-geometry finite volume algorithm for CFD analyses of unsteady incompressible flows using either URANS or LES approach for turbulence simulation. The capabilities and limitations of the code are demonstrated for different validation test cases.

2. NUMERICAL METHOD AND TURBULENCE SIMULATION

In an inertial frame of reference, the Reynolds Averaged Navier Stokes equations and the continuity equation for unsteady incompressible flow with moving boundaries may be written in tensor form as following using general non-orthogonal curvilinear coordinates where *j*, *k* and *m* as the summing indices; μ and ρ are the fluid viscosity and density respectively; p and $\overline{U}_i$ are the time-averaged pressure and cartesian velocity component respectively; u_i is the corresponding fluctuating velocity component due to turbulence and $\dot{v}_i$ is the grid velocity component indicating the motion of the body around which the flow is analysed. J is the transformation Jacobian between the cartesian and the curvilinear coordinates and β_j^i and B_j^i are the relevant geometric coefficients related to the transformation.

Momentum conservation :

$$\frac{\partial\left(\rho\overline{U}_i\right)}{\partial t}+\frac{1}{J}\frac{\partial}{\partial x_j}\left[\left(\rho\overline{U}_i(\overline{U}_k-\dot{v}_k)\beta_k^j\right)-\frac{\mu}{J}\left(\frac{\partial\overline{U}_i}{\partial x_m}B_m^j+\frac{\partial\overline{U}_k}{\partial x_m}\beta_i^m\beta_j^k\right)+p\beta_i^j+\rho\overline{u_iu_k}\beta_k^j\right]=0 \qquad (1)$$

Mass conservation :

$$\frac{\partial}{\partial x_j}\left(\rho(\overline{U}_k-\dot{v}_k)\beta_k^j\right)=0 \qquad (2)$$

The Reynolds stress tensor $-\rho\overline{u_iu_k}$ is evaluated through appropriate turbulence models. The Linear Eddy Viscosity (LEV) based models, most widely used in URANS computation of complex flows, assume the Reynolds stress tensor components to be directly proportional to the mean strain rates as follows :

$$-\rho\overline{u_iu_k}=\frac{\mu_t}{J}\left(\frac{\partial\overline{U}_i}{\partial x_n}\beta_k^n+\frac{\partial\overline{U}_k}{\partial x_m}\beta_i^m\right)-\frac{1}{3}\rho\delta_{ik}\overline{u_mu_m} \qquad (3)$$

where, δ_{ij} is the Kronecker Delta and the subscript *m* is a summation index. The eddy viscosity μ_t is evaluated from the relationship with the local turbulence scalars as following :

$$\mu_t=\rho C_\mu E_s T_s \qquad (4)$$

where E_s and T_s are appropriate energy scale and time scale respectively defining the local turbulence level, and C_μ is a model constant. Five different eddy viscosity based turbulence models are incorporated in the present URANS algorithm. The widely used *k*-ε model [10], *k*-ω model [26] and Shear Stress Transport model of Menter [17] assume $E_s=k$ and $T_s=k/\varepsilon$ or $1/\omega$ where k is the turbulence energy, ε the dissipation and ω the dissipation of turbulence energy. The Spalart-Allmaras model [24], on the other hand, solves a single transport equation for μ_t itself instead of using different scalars to evaluate μ_t. Another advanced LEV based model called V2F, proposed recently by Durbin [5], assumes $E_s=\overline{v^2}$ and $T_s=max\left[k/\varepsilon,6(\mu/\rho\varepsilon)^{1/2}\right]$ where $\overline{v^2}$ is a scalar representing the wall-normal component of the turbulence energy near the wall. The modeled transport equations for the relevant turbulence scalars, the closure coefficients, the special damping functions and additional terms for simulation of the near wall effects in *k*-ε model are described elsewhere [4] in details.

2.2 Governing Equations for the LES Approach

In LES approach, appropriate filtering operation [20] is first defined to decompose each flow variable Φ_i in the instantaneous NS equation into the sum of a filtered or resolved component ($\overline{\Phi}_i$) and a residual or subgridscale component (ϕ_i). The present algorithm uses a box filter as the filter kernel. The model filtered equations are solved numerically using the present time-accurate 3D finite volume algorithm using body-fitted curvilinear grids, where the unresolved residual stress tensor appearing in the resolved momentum equations is simulated by an eddy viscosity based turbulence model. In case of stationary grid under a general curvilinear coordinate system, the relevant momentum equation for the resolved velocity component $\overline{U}_i$ along *i* direction and the continuity equation are written as following where the other nomenclature has already been given in the previous subsection.

Mass conservation :
$$\frac{\partial}{\partial x_j}\left(\rho \overline{U}_k \beta_k^j\right) = 0 \tag{5}$$

Momentum conservation :
$$\frac{\partial\left(\rho\overline{U}_i\right)}{\partial t} + \frac{1}{J}\frac{\partial}{\partial x_j}\left[(\rho\overline{U}_i\overline{U}_k\beta_k^j) - \frac{\mu}{J}\left(\frac{\partial\overline{U}_i}{\partial x_m}B_m^j + \frac{\partial\overline{U}_k}{\partial x_m}\beta_i^m\beta_k^j\right) + p\beta_i^j - \tau_{ik}\beta_k^j\right] = 0 \tag{6}$$

The Residual or SubGrid Scale (SGS) stress tensor τ_{ik} may be expressed as the following:
$$\tau_{ik} = \rho(\overline{U}_i\overline{U}_k - \overline{U_iU_k}) \tag{7}$$

and this τ_{ik} needs to be modeled in order to close the filtered equations for $\overline{U}_i$. The SGS model proposed by Smagorinsky [23] is the simplest linear eddy viscosity based turbulence model where the residual stress (τ_{ik}) in Eq. 7 is related to the filtered rate of strain as following where the first and second term of the right hand side are the anisotropic and isotropic components respectively:
$$\tau_{ik} = \frac{\mu_{sgs}}{J}\left(\frac{\partial\overline{U}_i}{\partial x_m}\beta_m^k + \frac{\partial\overline{U}_k}{\partial x_m}\beta_i^m\right) - \frac{2}{3}\delta_{ik}k_{sgs} \tag{8}$$

μ_{sgs} is the eddy viscosity and k_{sgs} is the turbulence energy of the residual motions. The isotropic part is usually absorbed in the resolved pressure term and the anisotropic part is clubbed to the viscous diffusion term of Eq.(6) as following :
$$\frac{\partial\left(\rho\overline{U}_i\right)}{\partial t} + \frac{1}{J}\frac{\partial}{\partial x_j}\left[(\rho\overline{U}_i\overline{U}_k\beta_k^j) - \frac{(\mu+\mu_{sgs})}{J}\left(\frac{\partial\overline{U}_i}{\partial x_m}B_m^j + \frac{\partial\overline{U}_k}{\partial x_m}\beta_i^m\beta_k^j\right) + \left(p + \frac{2}{3}k_{sgs}\right)\beta_i^j\right] = 0 \tag{9}$$

The field values μ_{sgs} and k_{sgs} are computed through the following algebraic expressions based on mixing length hypothesis and used successfully by previous researchers [18,20]
$$\mu_{sgs} = \rho l^2\overline{S} = \rho(f_w C_s\Delta)^2\overline{S}\ ,\ k_{sgs} = \frac{\mu_{sgs}^2}{(\rho f_w C_k\Delta)^2}\ ;\ C_s = 0.1 \text{ and } C_k = 0.094 \tag{10}$$

where, $\overline{S}$ is the magnitude of the characteristic filtered rate of strain, *l* is the Smagorinsky mixing length, proportional to the filter width Δ, derived typically from the grid resolution as cube root of the volume of the control cell, C_s and C_k are closure coefficients and $f_w = 1 - exp(y^+/25)$ is a suitable Van Driest kind of damping function which allows the mixing length *l* to vary exponentially from zero at wall to $C_s\Delta$ in the turbulent boundary layer. Eqs. 5, 9 and 10 now form a closed set of equations to be solved for the resolved velocity components $\overline{U}_i$ and the resolved pressure *p* as function of space

and time. The mean resolved Reynolds stress components may then be evaluated from the time averaging of the correlation of corresponding resolved fluctuating velocity components $\overline{u_i}$ expressed as the difference between the instantaneous filtered velocity $\overline{U_i}$ and the time average of $\overline{U_i}$, obtained over a large number of time cycles after a statistically stationary state is reached.

2.3 Numerical Solution of Finite Volume Equation

The relevant Navier Stokes equations (Eq. 1 or Eq. 9) are first transformed to corresponding finite volume equations in terms of surface flux balance for each control volume using the Gauss Divergence theorem. An implicit predictor-corrector method based on a pressure-velocity solution strategy is used for numerical solution of the finite volume equation system. Second order accurate Central Difference or higher order low diffusion Upwind schemes are used for spatial discretisation of the convective fluxes whereas the temporal derivatives are discretised using the second order accurate three-level fully implicit scheme. Using the relevant geometric factors, appropriate discretisation schemes and linearisation of the source terms, the flux balance equations to be solved for momentum and turbulence scalars are expressed in a generalised implicit manner as follows at the predictor step:

$$\left(1.5\phi_P^{n+1} + 0.5\phi_P^{n-1} - 2\phi_P^{n}\right)\Delta V / \Delta t = \sum A_{nb}\phi_{nb}^{n+1} + SU - A_P\phi_P^{n+1} \qquad (11)$$

where $A_P = \sum A_{nb} - SP$; the coefficient A_{nb} represents the combined effect of convection and diffusion at the six faces of a hexahedral computational cell ; SU and SP are the components of the linearised source term, ΔV is the cell volume and Δt is the time step size. In the corrector step, the continuity equation is also transformed to a similar linearised equation for pressure correction in the form of Eq. 11. The corrections for pressure and velocity field obtained are added to the pressure and the momentum-satisfying velocities at the cell centers and cell faces, obtained at the predictor step. The derivation of Eq. 11 and the decoupled iterative procedure to handle the pressure-velocity link are given in details elsewhere [14, 15]. The system of linearised equations (Eq. 11) are solved at each outer iteration level using the strongly implicit procedure of Stone [25].

3. RESULTS AND DISCUSSION

3.1 Laminar flow past a bluff body mounted on the lower wall of a plane channel

This test case is chosen to demonstrate the predictive capability of the present URANS algorithm for non-periodic time-dependent laminar flows. In order to study unsteady flow separation on a bluff body mounted on the lower wall of a plane channel, flow visualization experiments have been conducted [1] using Laser Induced Fluoroscence (LIF) technique in a special water tunnel consisting of a two-component glass channel where the required flow velocity-time variation (Fig.1(a)) at the tunnel inlet is maintained by a servomotor system. The test plane is illuminated by a 2D Laser sheet and the image of the Fluorescent Sodium dye introduced on the body surface, is captured by a CCD camera at different instants of time during the piston motion. The URANS computation domain is bounded by the horizontal channel top wall, the test body geometry for the channel lower wall, an inflow and outflow plane at a distance of 8C on either side, where C is the channel height. Close view of the H-Grid (191×81) near the bluff body, used for computation is shown in Fig. 1(b). The algorithm uses central difference scheme for convective fluxes and second order time discretisation with time step size(Δt) of 0.002 units. Fig.1(c) compares the computed instantaneous streamlines to the flow visualization pictures at three different time instants starting from rest. Reasonably good agreement is observed between the computation and measurement for the instant and the location of the inception of unsteady flow separation and also for the size of the separation bubble growing with time.

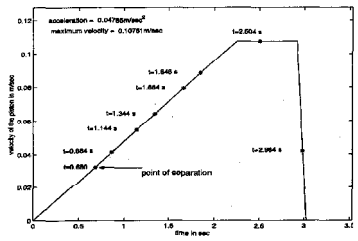

(a) Time-velocity variation in visualization study

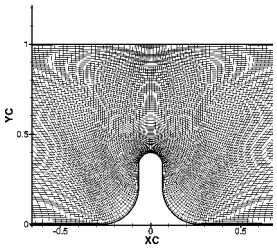

(b) Computational grid (191 × 81)

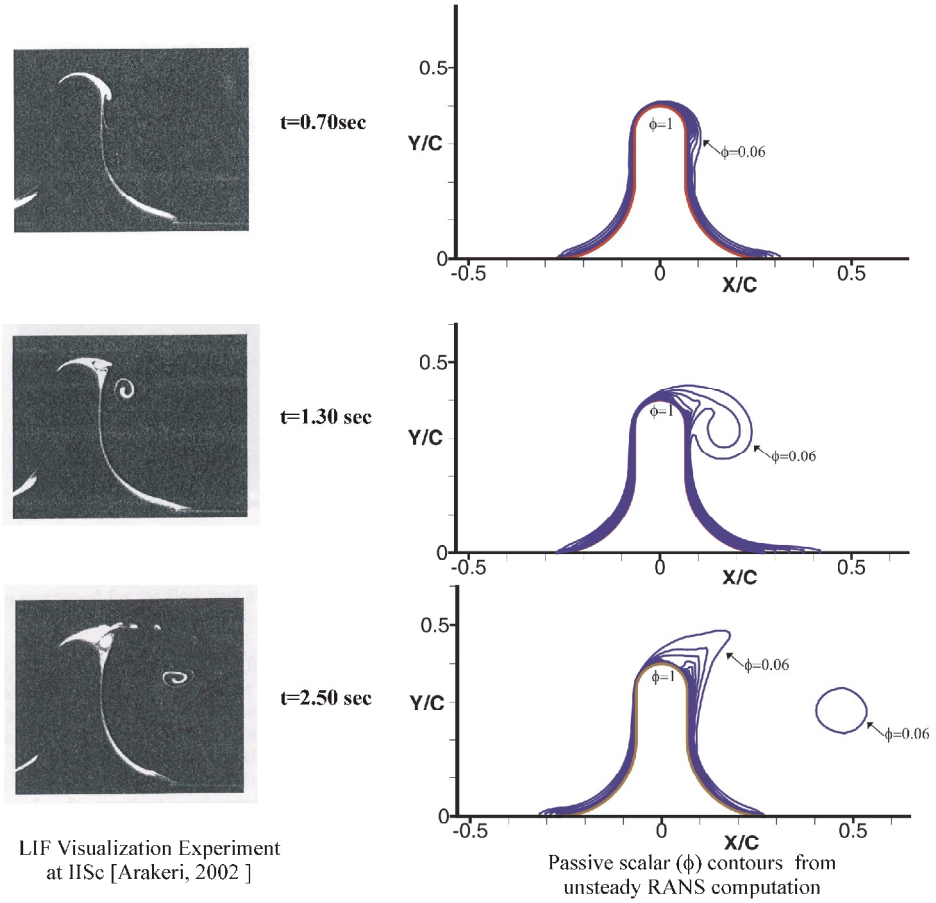

(c) Comparison between present computation and flow visualization experiment

Fig. 1 Unsteady laminar flow past a bluff body mounted on the lower wall of a channel

3.2 Turbulent Flow past a Pitching NACA 0012 Aerofoil

Flow past a pitching NACA0012 aerofoil is another example of a periodic unsteady flow caused by the sinusoidal motion of the aerofoil surface. This test case validates the accuracy and adequacy of the present URANS algorithm, specially with moving boundary conditions, against the measurement data of McAlister *et al* [16]. The aerofoil is subjected to a pitching motion about the quarter-chord point, defined as $\alpha = \alpha_o + 0.5(\alpha_1 - \alpha_o)(1 - cos\, kt)$ where $\alpha_o = 5^0$, $\alpha_1 = 25^0$ and $k(= \omega C/U_\infty) = 0.15$ is the reduced frequency of the oscillatory motion where ω is the physical frequency. A 2-block O-grid (Fig. 2(a)), consisting of 320 × 100 control volumes, has been employed with the far field placed at a radius of 15C and the minimum wall normal distance is maintained at around 8×10^{-6} C, where C is the chord length of the aerofoil. The third order accurate QUICK [11] scheme and second order accurate three-level implicit scheme have been used for spatial and temporal discretisation of convective fluxes. Fig. 2(b) shows the typical flow boundary conditions, where the farfield is treated either as an inflow or an outflow depending on the sign of the convective flux on the relevant face.

Convective boundary condition is used for outflow boundaries. Figs. 3 (a) and (b) show the instantaneous particle traces and the history of the surface pressure on the aerofoil at four different instants of the pitching cycle. The prediction [22] of the upper surface pressure agrees reasonably well with the measurement data [16] for different angles of attack encountered during the up and down stroke of the pitching motion of the aerofoil. At maximum value of α = 25^o, whole of the suction surface is observed to be covered by a large clockwise vortex with a small counter-clockwise vortex near the trailing edge which, during the downward motion, eventually pulls the large hysteresis vortex towards the trailing edge and hence reduces the vortex strength on the suction surface. As the value of α decreases during the downward motion, the large single vortex breaks into multiple small vortices, leading to sudden reduction of the suction pressure on the upper surface and hence to drastic loss of lift. Figs. 3(c) and (d) show the dynamic hysteresis loops for the lift and drag coefficients computed using different turbulence models. Results using the SA and SST turbulence models are observed to be in the better agreement with the measurement data. The double peaking of C_l during the start of the return downward stroke of the aerofoil, is reasonably captured by all the models. However quantitative

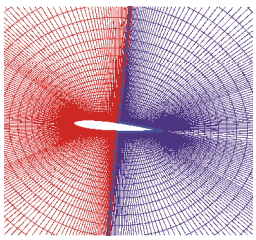

(a) Zoomed view of 2-block O-grid

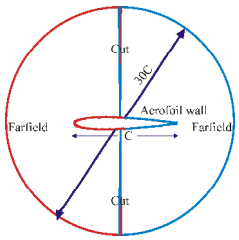

(b) Boundary condition for flow computation

Fig. 2 Grid and boundary condition used for aerofoil flow computation

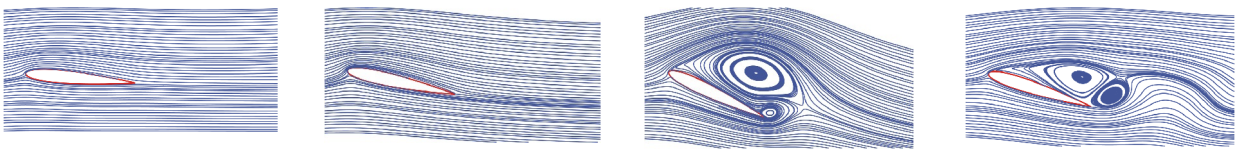

(a) Instantaneous particle trace

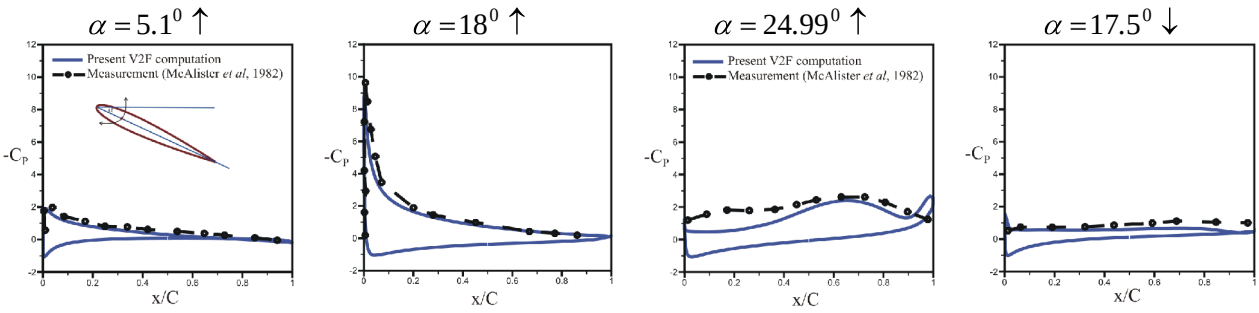

(b) Surface pressure distribution

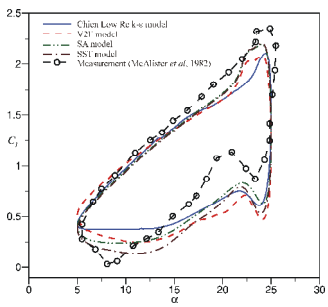

(c) Lift Coefficient

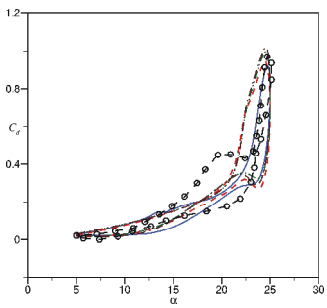

(d) Drag Coefficient

Fig. 3 Turbulent flow past a pitching NACA0012 aerofoil (Re=10^6, k=0.15 and Δt=0.05)

disagreement observed at some regions, may perhaps be attributed to the uncertainties and inadequacies of the eddy-viscosity based turbulence models used.

3.3 Turbulent flow past an Underwater Body with stern-end appendages

The main objective of selecting this steady flow problem is to demonstrate the capability of the multiblock parallel version of the present URANS algorithm even for prediction of steady three-dimensional turbulent flow past any complex arbitrary shaped geometry. This problem is about prediction of three-dimensional turbulent flow around an axisymmetric hull of the DARPA Suboff model of submarine consisting of a forebody, a parallel midbody section and an afterbody with four radial fins of NACA0020 aerofoil cross- section attached at the stern end of the hull. Detailed hot-film anemometer measurements are reported [7] for this case from the David Taylor Model Basin Research Group,USA. A differential-algebraic grid generation procedure developed at the CTFD Division, NAL [21] is employed to generate structured, boundary-fitted grid required for the present problem. The computational domain is divided into 24 blocks, 4 along the circumferential and 6 along the longitudinal direction (Fig.4(a)). A H-O grid topology is used with total number of 245 Control Volumes (CV) along longitudinal, 80 CV along radial and 82 CV along tangential directions. A close view of the surface grid near the hull-fin intersection is shown in Fig. 4(b). The present prediction [15]

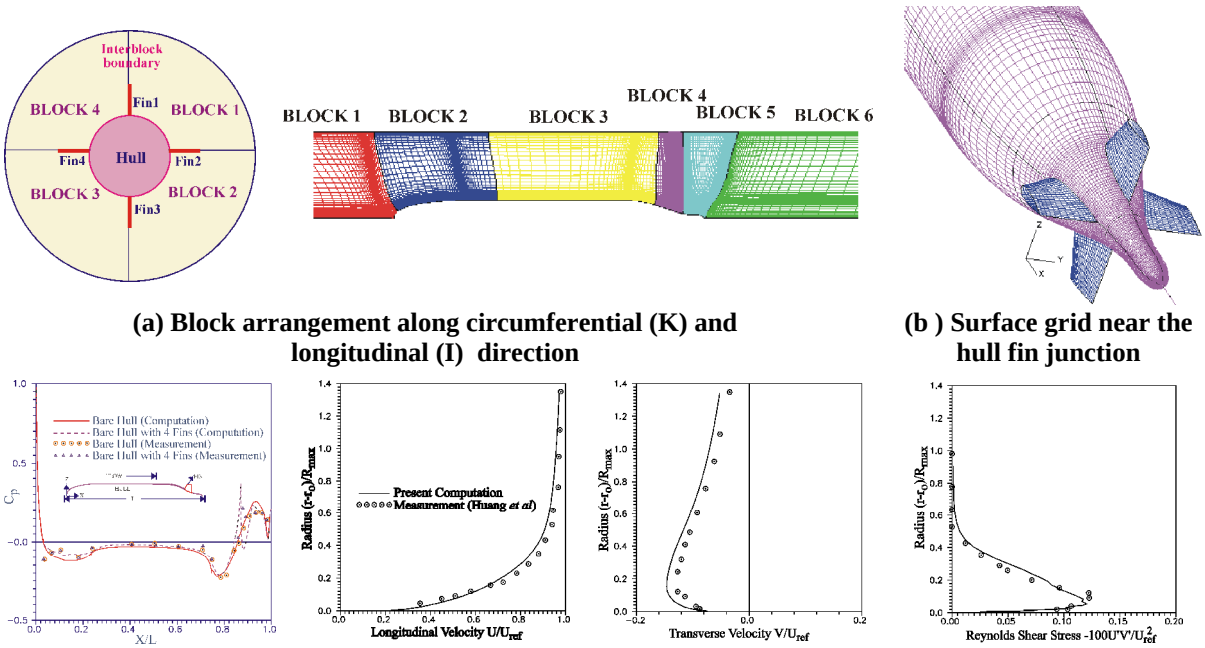

(a) Block arrangement along circumferential (K) and longitudinal (I) direction

(b) Surface grid near the hull fin junction

(c) Surface pressure on a vertical meridional plane

(d) Transverse profiles of mean velocity and Reynolds shear stress

Fig. 4 Turbulent flow around a DARPA Suboff with stern-end appendages ($Re=1.2x10^7$)

is compared in Fig.4(c) with the measurement data for surface pressure along the vertical meridional plane of the hull with fins. The disagreement between computation and measurement data near the stern end, may be attributed partly to the inaccuracy in the geometry-prescription near the strong curvature zone of the stern end and partly to the well known inadequacy of the k-ε models in the adverse pressure gradient region. The present prediction is also compared to the measurement data [7] (Fig. 4 (d)) for the transverse profiles of the mean longitudinal velocity and the Reynolds shear stress for the bare hull at a longitudinal station X/L = 0:904 and the agreement is observed to be reasonably good.

3.4 Turbulent flow past a Ship Hull with Bow-mounted Sonar Dome

This is an interesting example of ship viscous flow which is assumed to be steady and also symmetric around the vertical midplane of the configuration. This turbulent flow problem for very complex geometry is predicted using the present URANS algorithm and validated against corresponding measurement data on the drag forces on the dome surface only, obtained from a towing tank test on a scaled down model of the configuration. The geometry of the hull with bow-mounted sonar dome is specified by NSTL, Visakhapatnam and a differential-algebraic hybrid grid generation methodology is used to generate a stacked quasi-3D grid consisting of vertical parallel planes in the form of a H-O grid topology (109 ×109× 65). Flow computations have been carried out for three different hull speed of 7, 15 and 30 knots and detailed results are documented in another report [9]. The stretching factor and number of grids along transverse direction are so chosen that the near wall distance in wall coordinates (y^+) is always maintained between 30 and 100, as requirement of the logarithmic law of wall for the near wall zone. Second-order accurate Central Difference scheme (CDS) coupled to the deferred correction procedure [8] combining 10% of Upwind fluxes and 90% of CDS fluxes is used for the computation. The free stream turbulence level and the eddy viscosity are assumed to be 1% and 10 times the laminar viscosity respectively.

(a) View of the hull model with sonar dome for resistance test at NSTL towing tank

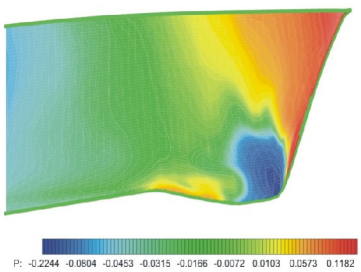

(b) Pressure contours on hull surface

(c) Longitudinal velocity contours and particle trace on cross plane at X/L=0.0794

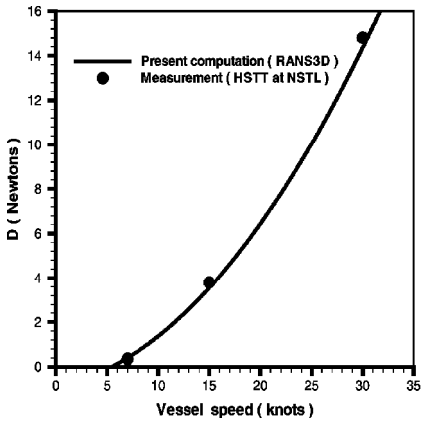

(d) Variation of drag force on the sonar dome with vessel speed

Fig . 5 Turbulent flow around a ship hull with bow-mounted sonar dome (Vessel Speed = 30 knots)

In order to validate the present computation results, resistance tests have been carried out for the hull model in the High Speed Towing Tank at NSTL Visakhapatnam. The tests have been conducted at NSTL on 1/24th scaled down Fiber Reinforced Plastic (FRP) models. The model is tested for the bare hull resistance characteristics corresponding to a full scale draft of 5.05m. The model is towed using R-47 dynamometer attached to the carriage. The photograph of the hull model with the sonar dome as an integral part is shown in Fig. 5(a). For the purpose of code validation, the sonar dome is physically separated from the hull by cutting the model at appropriate location of the dome. The separated dome portion of the hull is connected to the towing carriage through a load cell for measurement of

horizontal forces. The dome is connected to the hull by means of flexible watertight nylon strips which do not allow any transmission of forces to the remaining part of the hull during the test. Computed surface pressure contours over the hull surface at a vessel speed of 30 knots are shown in Fig. 5(b). In the zone very close to the bow end, the flow, in general, bends smoothly along the hull surface after hitting the bow end edge as a stagnation line. In the stream wise direction the flow is observed to remain attached all through the length of the hull considered. The high-pressure region near the stagnation line and the low-pressure zone near the bulge of the sonar dome due to local acceleration are clearly visible in the surface pressure contours. The contours of longitudinal velocity (U/U_{vessel}) and the cross flow pattern as particle traces using the cross-stream velocity components only are shown in Fig. 5(c) at a typical dome cross-section of X/L=0.0794 where the bulge due to the dome is maximum. The cross flow pattern also shows how the flow separates near the keel leading to the formation of tiny vortices. Fig. 5(d) compares the computed drag force on the sonar dome surface to the corresponding towing tank measurement data directly in Newtons, for three different vessel speeds. Reasonable agreement, observed between the computed results and the measurement data confirms the adequacy of the mathematical modeling and the numerical accuracy of the present URANS algorithm used for the computation of the three-dimensional turbulent flow field past a ship hull.

3.5 LES for Turbulent flow past a Circular Cylinder at Re=3900

This is a classic example of an unsteady three-dimensional flow consisting of separation, reattachment, three dimensionalities, free shear layer instabilities, laminar to turbulent transition and vortex shedding in the cylinder wake. Since the URANS approach with eddy viscosity-based turbulence model are reported [2, 3, 6] to be inaccurate and unreliable for transitional flows, this test flow is identified as the ideal candidate for validation of the LES methodology. A four block cylindrical polar grid is used to cover the annular computation domain formed by a unit diameter cylinder, the far field circular boundary at a radius of 20 units and a spanwise length of 2π units. The computation domain covering $120 \times 145 \times 30$ control volumes has been decomposed into four blocks to be computed in parallel using four processors of an SGI Altix machine, each processor covering one quarter segment of the cylinder along the circumferential direction (Fig. 6(a)). No slip condition is used on the wall surface, whereas the far field boundaries are treated as inflow or outflow depending on the sign of the local mass flux. The spanwise end planes are treated as periodic boundaries. The computation using a timestep size of 0.05 units, takes about 6 clock hours to reach a statistically stationary state. Grids are equispaced along circumferential and spanwise direction, and stretched radially near the cylinder wall for fine resolution of the boundary layer. A low sub-critical Reynolds number of 3900 is chosen for which the measurement data show that the flow separation on cylinder wall is laminar and the transition to turbulence takes place in the free shear layers. Once a statistically stationary state is reached, computation is continued further and the value of the flow variables are averaged over number of time steps required to cover at least 30 vortex shedding cycles and also averaged over the spanwise direction for comparison to measurement data [12,13, 19] on the midspan plane ($z=0$). Fig. 6(b) shows the computed isosurfaces of the instantaneous vorticity magnitude $\left(|\omega| D/U_\infty\right)$ in the cylinder wake for fourteen different values ranging from 0.5 to 10. The figure clearly demonstrates the two free shear layers formed following the flow separation from the cylinder surface and also the complex three-dimensional wake structure developed due to the interaction between the shear layers and the primary Karman vortex street behind the cylinder. Further, two isosurfaces of streamwise components of vorticity $\left(\omega_x D/U_\infty = \pm 0.7\right)$ of equal magnitude with opposite signs, represented by two different colours in Fig.6 (c), demonstrate the flow structures consisting of streamwise vortices of alternating signs along the spanwise direction, typically formed in three-dimensional flows over a finite span. Figs. 6(d) and (e) show reasonable agreement between the measurement data and the present 3D LES computation results (both with and without SGS model) for the circumferential variation of the average surface pressure and also for the variation of the mean streamwise velocity along the wake centerline. On the other hand, the 2D LES with no model clearly fails to predict the attached recirculation region behind the cylinder, observed in measurement data and yields inaccurate results for the surface pressure variation as well. Figs. 6(f) to 6(i) compare the present LES predictions and the corresponding measurement data for the transverse profiles of the mean streamwise velocity

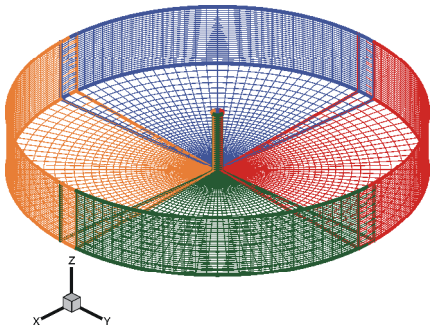

(a) Surface Grids for 4-block configuration

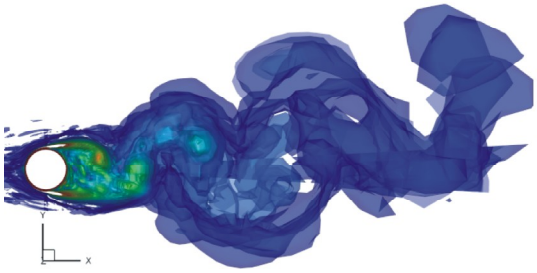

(b) Isosurfaces of instantaneous vorticity magnitude

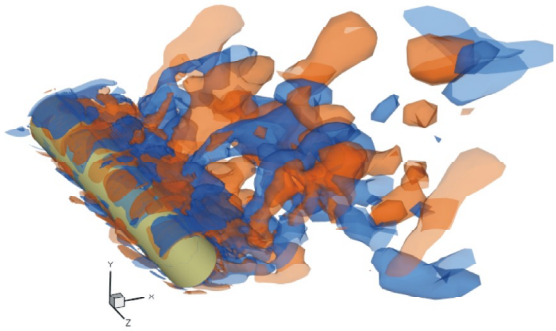

(c) Isosurfaces of instantaneous streamwise vorticity component

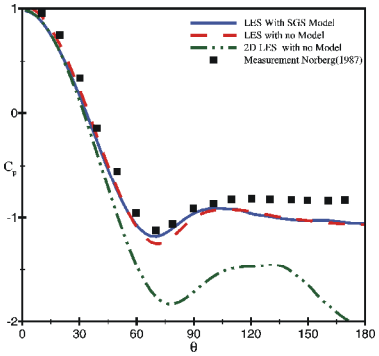

(d) Mean surface pressure coefficient around the cylinder

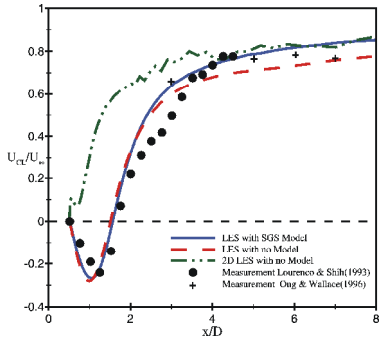

(e) Mean resolved streamwise velocity at wake centerline

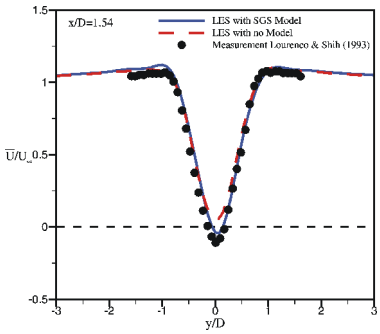

(f) Transverse Profile of mean resolved streamwise velocity

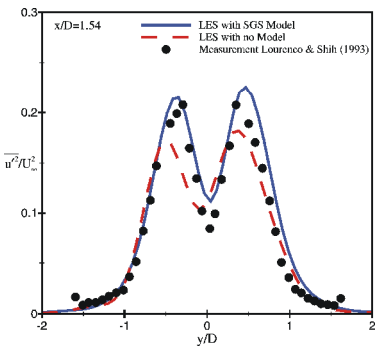

(g) Streamwise component of resolved Reynolds stress

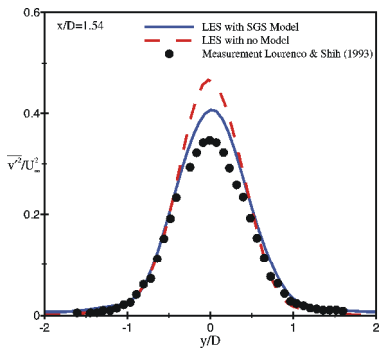

(h) Cross-stream component of resolved Reynolds stress

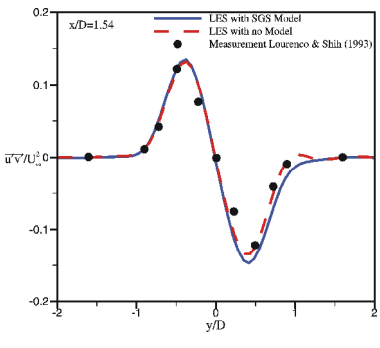

(i) Shear component of resolved Reynolds stress

Fig. 6 Large Eddy Simulation of Turbulent flow past a Circular Cylinder at Re=3900

component and three different components of the total resolved Reynolds stress at the longitudinal station x/D=1.54. Reasonable agreement is observed for all the flow quantities between the measurement data and the present LES computation results. Better agreement observed between

measurement data and LES results with SGS model indicates the significant effect of the SGS model to capture the momentum and energy transport mechanism between the resolved large scale structures and the small subgrid scale eddies for the chosen grid size, even at moderately low Re value of 3900.

4. CONCLUDING REMARKS

A fully implicit second order accurate pressure-based Navier Stokes solver in generalised body-fitted non-orthogonal coordinate system, has been developed at the CTFD Division, NAL, Bangalore, for time-accurate calculation of incompressible turbulent flow in or around arbitrary shaped configurations. The simulation of turbulence may be carried out using either URANS or LES approach to be chosen by the user. The algorithm is also parallelised efficiently using the domain decomposition method, coupled to multiblock structured grid for handling complex configuration. The code validation studies have demonstrated the accuracy and adequacy of the spatial and temporal discretisation schemes used, the handling of moving boundaries in an inertial frame of reference and the proper implementation of parallelisation of the algorithm in a multiblock structured grid environment. For turbulent flows, the URANS approach coupled to variety of linear eddy viscosity based turbulence models with special near wall treatments are found to be reasonably accurate for prediction of turbulent boundary layer flows with mild flow separation under moderate adverse pressure gradients. The superior performance of LES approach for more realistic and accurate simulation of turbulence physics for complex flows in presence of transition, flow unsteadiness, strong effects of curvature or rotation, has been established through the example of flow past a circular cylinder. Work is in progress to incorporate Non-Linear Eddy Viscosity based models for URANS and Dynamic SGS models for LES computations to achieve better accuracy. Capabilities of the code are being further enhanced to handle multiphysics problems in future incorporating models for multiphase flow, free-surface flow and reacting flows.

ACKNOWLEDGEMENTS

The authors wish to thank the Director NSTL(DRDO), and the Hydrodynamics Panel of the Naval Research Board for the financial support provided to this development work through several research projects sponsored to NAL(CSIR). The authors also wish to thank the Director NAL (CSIR) for his kind permission to publish this paper.

REFERENCES

1) Arakeri, J. H. (2002). *Naval Research Board Project Report*, ME Deptt., IISc., Bangalore
2) Beaudan P., Moin P. (1994), *Report TF62,* Mech. Engg. Department, Stanford University
3) Breuer, M. (1998), *International Journal of Heat and Fluid Flow,* vol. 19, pp. 512-521
4) Chien K.Y (1982) *AIAA Journal*, vol. 20, no. 1, pp. 33-38
5) Durbin, P. A. (1995), *AIAA Journal*, vol.33, pp. 659-664
6) Franke R., Rodi W. (1991), *Proc. 8th Turbulent Shear Flows Symposium,* p.189
7) Huang, T., *et al.* (1994), *Proc. 19th Symp. on Naval Hydrodynamics*
8) Khosla, P. K. , Rubin, S. G. (1974), *Computers and Fluids,* vol.2 pp.207-209.
9) Kulkarni D.S., Rajani B., Majumdar S. (2003), *NAL PD CF 0313*
10) Launder B.E., Spalding D.B. (1974), *Comp. Methods in App .Mech. and Engg*., vol. 3, pp.269
11) Leonard B. P. (1979), *Comp. Methods in App. Mech.and Engg*., vol.19, pp. 59-98
12) Lourenco L.M *et al*.(1993), ref. M. Breuer, *Int. J. of Heat & Fluid Flow*, vol. 21, pp. 648-654
13) Norberg, C.(1987), *Report 87/2, App.Therm.& Fluid Mech,.Chalmer Univ.,Gothenburg*
14) Majumdar S., Rodi W., Zhu J. (1992), *Journal of Fluid Engineering., ASME*, pp. 496-503
15) Majumdar S. *et al* (2003), *NAL SP 0301*, pp. 31-48
16) McAlister K.W. *et al* (1982), *NASA TM-84245,* vol.2, Sept. 1982

17) Menter F.R.(1994), *AIAA Journal*, vol. 32, no.8, pp. 1598-1605
18) Murakami S., Mochida S.(1995), *Journal of Wind Engg. & Indust. Aero 54/55*, pp. 191-211
19) Ong L., Wallace J. (1996), *Experiments in Fluids*, vol. 20, Springer Verlag, pp. 441-453
20) Piomelli U. (1994), *Theo. & Appl. Mechanics (TAM) Report No. 767*, UILU-ENG-94-6023
21) Rajani B.N.,Majumdar S.,.(1997), *Proc. Ship & Ocean Technology* (SHOT97), IIT Kharagpur
22) Rajani B.N., Govindaraju L., Majumdar S.(2007), *Proc. 7th Asian CFD Conference, Bangalore*
23) Smagorinsky J. (1963), *Mon. Weather Review*, vol. 91, pp. 99-165
24) Spalart, P.R., Allmaras, S.R. (1992), *AIAA Paper 92-0439*
25) Stone H.L.(1968) *SIAM Journal of Numerical Analysis*, vol. 5, pp. 530-538
26) Wilcox D.C. (1993) *Turbulence Modeling for CFD*, DCW Industries, Inc., California